PNAS RESEARCH ARTICLE | NEUROSCIENCE OPEN ACCESS

Misregulation of mitochondria–lysosome contact dynamics in Charcot–Marie–Tooth Type 2B disease Rab7 mutant sensory peripheral neurons

Yvette C. Wong[a,1,2], Nirupa D. Jayaraj[a,1], Tayler B. Belton[a], George C. Shum[a], Hannah E. Ball[a], Dongjun Ren[a], Abigail L. D. Tadenev[b], Dimitri Krainc[a,c], Robert W. Burgess[b], and Daniela M. Menichella[a,d,2]

Edited by Nancy Bonini, University of Pennsylvania, Philadelphia, PA; received August 4, 2023; accepted September 12, 2023

Inter-organelle contact sites between mitochondria and lysosomes mediate the crosstalk and bidirectional regulation of their dynamics in health and disease. However, mitochondria–lysosome contact sites and their misregulation have not been investigated in peripheral sensory neurons. Charcot–Marie–Tooth type 2B disease is an autosomal dominant axonal neuropathy affecting peripheral sensory neurons caused by mutations in the GTPase Rab7. Using live super-resolution and confocal time-lapse microscopy, we showed that mitochondria–lysosome contact sites dynamically form in the soma and axons of peripheral sensory neurons. Interestingly, Charcot–Marie–Tooth type 2B mutant Rab7 led to prolonged mitochondria–lysosome contact site tethering preferentially in the axons of peripheral sensory neurons, due to impaired Rab7 GTP hydrolysis–mediated contact site untethering. We further generated a Charcot–Marie–Tooth type 2B mutant Rab7 knock-in mouse model which exhibited prolonged axonal mitochondria–lysosome contact site tethering and defective downstream axonal mitochondrial dynamics due to impaired Rab7 GTP hydrolysis as well as fragmented mitochondria in the axon of the sciatic nerve. Importantly, mutant Rab7 mice further demonstrated preferential sensory behavioral abnormalities and neuropathy, highlighting an important role for mutant Rab7 in driving degeneration of peripheral sensory neurons. Together, this study identifies an important role for mitochondria–lysosome contact sites in the pathogenesis of peripheral neuropathy.

Charcot–Marie–Tooth disease | inter-organelle contact site | peripheral neuropathy | mitochondria | lysosome

Charcot–Marie–Tooth disease is the most common genetic form of peripheral neuropathy (1, 2), with Charcot–Marie–Tooth type 2 encompassing autosomal dominant forms of the disease that result in axonal degeneration. In particular, Charcot–Marie–Tooth type 2B is caused by autosomal dominant GTPase Rab7 mutations (3–8), which lead to defective GTP (guanosine 5′-triphosphate) hydrolysis and increased GTP binding (9–11). Of note, Charcot–Marie–Tooth type 2B results in the axonal degeneration of peripheral sensory neurons, leading to sensory behavioral abnormalities (3–7). However, the molecular mechanisms underlying the etiology of Charcot–Marie–Tooth type 2B mutant Rab7 in peripheral sensory neurons are still not completely understood.

Mitochondria–lysosome contact sites were recently identified as a critical pathway for bidirectional crosstalk between mitochondria and lysosomes (12–14). These inter-organelle contact sites dynamically form between mitochondria and lysosomes (12, 15) and further mediate the lysosomal regulation of mitochondrial dynamics (12, 16, 17). Importantly, mitochondria–lysosome contact untethering is driven by Rab7 GTP hydrolysis at contact sites (12, 13). However, whether Charcot–Marie–Tooth type 2B mutant Rab7 disrupts mitochondria–lysosome contact dynamics in peripheral sensory neurons is not known as well as whether this drives axonal defects in disease. Moreover, how this contributes to defects in mitochondrial dynamics was previously unclear and has important implications for elucidating the pathways underlying Charcot–Marie–Tooth disease. Finally, whether Charcot–Marie–Tooth type 2B mutant Rab7 in vivo mouse models also exhibit preferential sensory behavioral deficits has never been studied and will help to shed light on the pathogenesis of Charcot–Marie–Tooth type 2B disease.

Using live super-resolution and confocal time-lapse microscopy, we found that mitochondria–lysosome contact sites dynamically formed in the soma and axons of peripheral sensory neurons. Interestingly, Charcot–Marie–Tooth type 2B mutant Rab7 led to prolonged mitochondria–lysosome contact site tethering dynamics, preferentially in the axons of peripheral sensory neurons, which was rescued by targeting Rab7 GTP hydrolysis machinery to promote mitochondria–lysosome contact untethering events. We further

Significance

Charcot–Marie–Tooth disease is the most common genetic peripheral neuropathy, with autosomal dominant mutations in Rab7 causing Charcot–Marie–Tooth type 2B disease, which is characterized by the axonal degeneration of peripheral sensory neurons. However, the mechanistic pathways underlying disease pathogenesis are still not completely understood. This study demonstrates a key role for dynamic mitochondria–lysosome contact sites in peripheral sensory neurons, and elucidates their preferential misregulation in axons of Charcot–Marie–Tooth type 2B disease Rab7 neurons. Contact site dynamics are further disrupted in peripheral sensory neurons from a Charcot–Marie–Tooth type 2B mouse model which exhibits deficits in downstream mitochondrial dynamics and ultimately undergoes sensory behavioral abnormalities and neuropathy. This work highlights an important pathway for mutant Rab7 in driving sensory peripheral neuropathy.

This article is a PNAS Direct Submission.

[1]Y.C.W. and N.D.J. contributed equally to this work.

[2]To whom correspondence may be addressed. Email: yvette.wong@northwestern.edu or d-menichella@northwestern.edu.

This article contains supporting information online at https://www.pnas.org/lookup/suppl/doi:10.1073/pnas.2313010120/-/DCSupplemental.

Published October 25, 2023.

generated a Charcot–Marie–Tooth type 2B mutant Rab7 knock-in mouse model, which exhibited defective lysosomal morphology consistent with Rab7's known role in this pathway. Importantly, peripheral sensory neurons from Rab7 disease mutant mice further recapitulated defective axonal mitochondria–lysosome contact dynamics leading to downstream defects in mitochondrial dynamics, both of which could be rescued by targeting Rab7 GTP hydrolysis machinery. Finally, Charcot–Marie–Tooth type 2B mutant Rab7 mice exhibited preferential sensory behavioral abnormalities, highlighting an important role for mutant Rab7 in driving peripheral sensory neurodegeneration. Together, this study identifies a critical role for mitochondria–lysosome contact sites in sensory peripheral neurons contributing to the peripheral neuropathy in Charcot–Marie–Tooth type 2B.

Results

Mitochondria–Lysosome Contact Sites Dynamically Form in Peripheral Sensory Neurons. To investigate the dynamics of mitochondria–lysosome contact sites in peripheral sensory neurons, we conducted live time-lapse confocal microscopy of mitochondria and lysosomes from primary mouse dorsal root ganglion (DRG) neurons. Both mitochondria and lysosomes could be visualized in the soma (Fig. 1*A*) and were found to form mitochondria–lysosome contact sites which remained dynamically tethered together over time (white arrows; Fig. 1*B*). Of note, mitochondria and lysosomes were separate from one another pre-contact (Fig. 1*C*), before subsequently tethering together at a contact site (Fig. 1*D*). Indeed, multiple mitochondria–lysosome contact sites dynamically tethered at any one time within a single soma (*SI Appendix*, Fig. S1 *A–C*). We further investigated contact formation in axons, and again visualized both mitochondria and lysosomes within axons (Fig. 1*E*). Importantly, mitochondria–lysosome contact sites also formed within axons of peripheral sensory neurons (white arrows; Fig. 1*F*), which dynamically formed and remained tethered in contact (Fig. 1 *G* and *H*). Multiple mitochondria–lysosome contacts could also be dynamically tethered within a single axon (*SI Appendix*, Fig. S1 *D–F*). Super-resolution Airyscan2 live microscopy of photoactivated mitochondria further demonstrated the formation of mitochondria–lysosome contact sites in peripheral sensory neurons (*SI Appendix*, Fig. S2 *A* and *B*). Thus, mitochondria and lysosomes can form dynamic inter-organelle contact sites in peripheral sensory neurons.

We next analyzed the dynamics of mitochondria–lysosome contact site tethering. Contacts lasted between 60 s and >300 s in peripheral sensory neurons (Fig. 1*I*), with an average tethering duration of ~180 s (Fig. 1*J*). Of note, ~25% of lysosomes formed a contact with mitochondria at any point in time (Fig. 1*K*). Moreover, mitochondria–lysosome contact tethering duration was similar in both soma and axons (Fig. 1*L*). Indeed, the percent of lysosomes forming contacts with mitochondria (*SI Appendix*, Fig. S1*G*) and mitochondria–lysosome contact tethering duration (*SI Appendix*, Fig. S1*H*) was not altered between soma and axons in peripheral sensory neurons. Thus, mitochondria–lysosome contact sites dynamically form in both soma and axons of peripheral sensory neurons over time.

Misregulation of Mitochondria–Lysosome Contacts in Charcot–Marie–Tooth Type 2B Mutant Rab7 Peripheral Sensory Neuron Axons. To investigate whether Charcot–Marie–Tooth type 2B mutant Rab7 misregulated mitochondria–lysosome contact dynamics in peripheral sensory neurons, we expressed either Rab7(WT) or the most common Charcot–Marie–Tooth type 2B disease-linked Rab7 (V162M) mutation in neurons (3, 7). Live time-lapse confocal microscopy of mitochondria and lysosomes was subsequently conducted in the soma and axons of Rab7(WT) neurons (*SI Appendix*, Fig. S3 *A* and *B*) and Rab7(V162M) neurons (*SI Appendix*, Fig. S3 *C* and *D*).

Of note, super-resolution microscopy further revealed mitochondria–lysosome contact sites in both Rab7(WT) and Rab7(V162M) peripheral sensory neurons, using super-resolution Airyscan2 imaging of the mitochondrial matrix (*SI Appendix*, Fig. S4 *A–D*) and the outer mitochondrial membrane (*SI Appendix*, Fig. S5 *A* and *B*), and super-resolution Lattice SIM^2 (structured illumination microscopy) (*SI Appendix*, Fig. S5 *C* and *D*). In addition, proximity ligation assay studies of the outer mitochondrial membrane (TOM20) and the lysosomal membrane (LAMP1) (*SI Appendix*, Fig. S6 *A–D*) further demonstrated that mitochondria–lysosome contact sites could form in both Rab7(WT) and Rab7(V162M) peripheral sensory neurons.

Importantly, while Rab7(V162M) did not disrupt the percentage of lysosomes in contact with mitochondria (Fig. 2*A*), it led to a significant increase in the tethering duration of mitochondria–lysosome contact sites in peripheral sensory neurons (***$P < 0.001$; Fig. 2*B*). Rab7 GTP hydrolysis normally drives the conversion of active GTP-bound Rab7 on lysosomal/late endosomal membranes to an inactive GDP-bound Rab7 which returns to the cytosol (18). However, Charcot–Marie–Tooth mutant Rab7(V162M) has been shown to disrupt Rab7 GTP hydrolysis, leading to its prolonged and more stably bound active GTP-state on lysosomal/late endosomal membranes and preventing its return to the cytosol (9–11). We thus further investigated whether Rab7(V162M) dynamics were defective in peripheral sensory neurons. Using super-resolution Airyscan2 fluorescence recovery after photobleaching (FRAP) imaging, photobleaching of Charcot–Marie–Tooth mutant Rab7(V162M) demonstrated that it was more stably bound to lysosomes in contact with mitochondria, as compared to Rab7(WT) (*SI Appendix*, Fig. S7 *A* and *B*). Importantly, Rab7(V162M) further showed significantly reduced FRAP recovery rates back to the lysosomal membrane, including for lysosomes in contact with mitochondria (*SI Appendix*, Fig. S7 *D* and *E*), further demonstrating that Rab7 GTP hydrolysis is disrupted by Charcot–Marie–Tooth mutant Rab7(V162M) at mitochondria–lysosome contact sites. Together, these findings are consistent with a role for Rab7 GTP hydrolysis in driving mitochondria–lysosome contact untethering events (12, 13), which is disrupted by Charcot–Marie–Tooth type 2B mutant Rab7 in peripheral sensory neurons.

As Charcot–Marie–Tooth type 2B leads to axonal degeneration in peripheral sensory neurons, we then interrogated whether mitochondria–lysosome contact site dynamics might be preferentially disrupted in axons of Rab7(V162M) neurons. Indeed, we found that while contacts untethered by 160 s in axons from Rab7(WT) neurons (yellow arrow; Fig. 2*C*), mitochondria–lysosome contacts remained tethered even after 200 s in axons from Rab7(V162M) neurons (white arrow; Fig. 2*D*), suggesting that Rab7(V162M) disrupted contact site untethering in axons. In contrast, mitochondria–lysosome contacts tethered with similar dynamics in the soma of Rab7(WT) neurons (*SI Appendix*, Fig. S8 *A–D*) and Rab7(V162M) neurons (*SI Appendix*, Fig. S8 *E–H*). Indeed, detailed quantification of mitochondria–lysosome contact site dynamics demonstrated that while the percentage of lysosomes in contact with mitochondria was not disrupted by Rab7(V162M) in either soma or axons (Fig. 2 *F* and *G*), the tethering duration of mitochondria–lysosome contact sites in peripheral sensory neurons was preferentially prolonged in axons by Rab7(V162M) but not in the soma (***$P < 0.001$; Fig. 2 *H* and *I*). Thus, Charcot–Marie–Tooth mutant Rab7 preferentially disrupts mitochondria–lysosome contact tethering dynamics in the axons of peripheral sensory neurons.

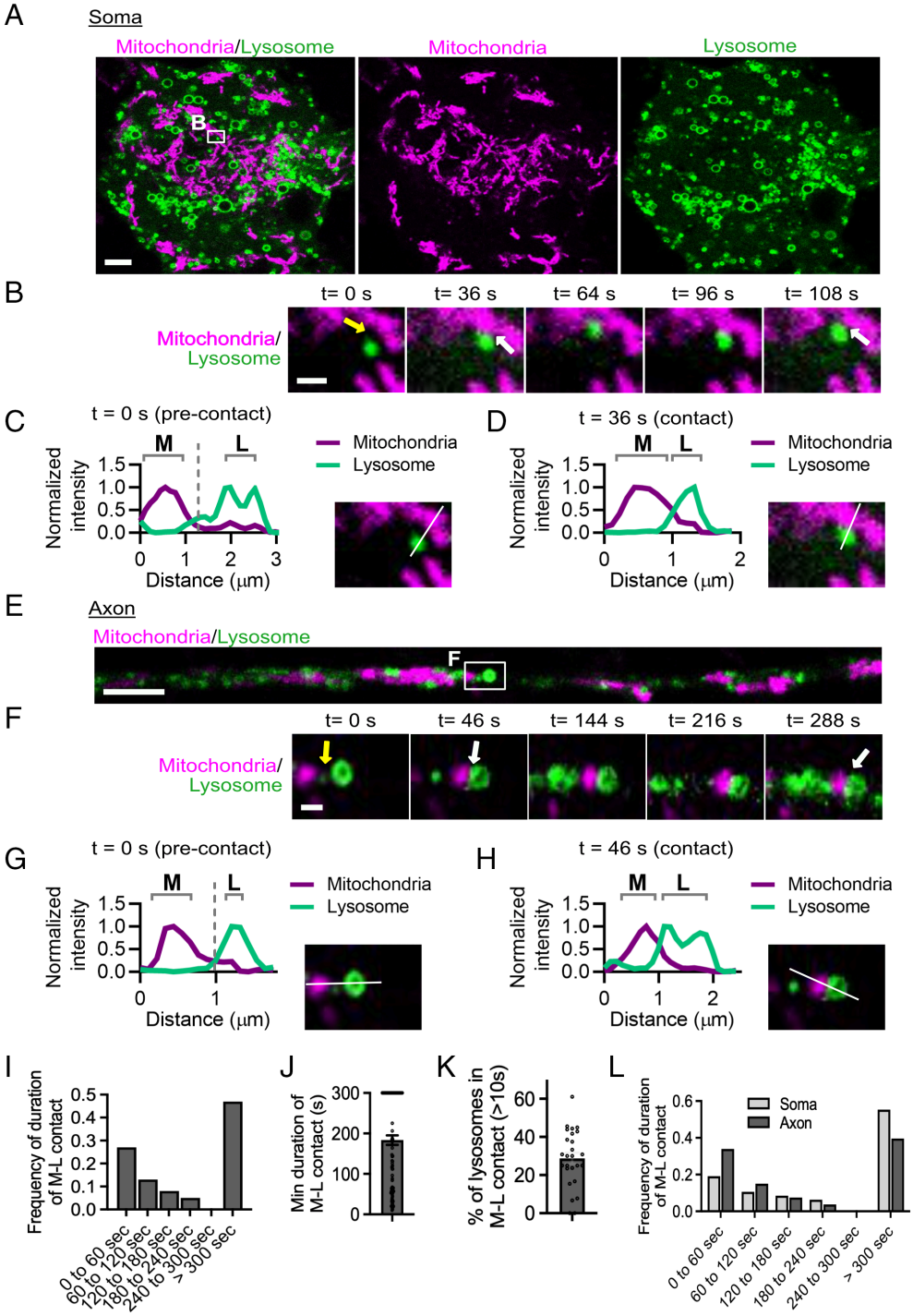

Fig. 1. Mitochondria–lysosome contact sites dynamically form in the soma and axons of peripheral sensory neurons. (*A*) Confocal live microscopy image of mitochondria and lysosomes in the soma of peripheral sensory neurons [Mitochondria: MitoTracker Red; Lysosome: mNeonGreen-Rab7(WT)]. (Scale bar: 5 μm.) (*B*) Confocal live microscopy time-lapse images of mitochondria–lysosome contact site formation in soma of peripheral sensory neurons (yellow arrow, pre-contact; white arrow, contact tethered). (Scale bar: 1 μm.) (*C*) Linescan of mitochondria and lysosome pre-contact (t = 0 s), corresponding to Fig. 1*B*. (*D*) Linescan of mitochondria and lysosome tethered at contact site (t = 36 s), corresponding to Fig. 1*B*. (*E*) Confocal live microscopy image of mitochondria and lysosomes in the axon of peripheral sensory neurons. (Scale bar: 5 μm.) (*F*) Confocal live microscopy time-lapse images of mitochondria–lysosome contact site formation in the axon of peripheral sensory neurons (yellow arrow, pre-contact; white arrow, contact tethered). (Scale bar: 1 μm.) (*G*) Linescan of mitochondria and lysosome pre-contact (t = 0 s), corresponding to Fig. 1*F*. (*H*) Linescan of mitochondria and lysosome tethered at contact site (t = 46 s), corresponding to Fig. 1*F*. (*I* and *J*) Histogram and quantification of mitochondria–lysosome contact site tethering minimum duration in peripheral sensory neurons. (n = 100 events from 13 neurons). (*K*) Quantification of percentage of lysosomes forming mitochondria–lysosome contact sites in peripheral sensory neurons. (n = 14 neurons). (*L*) Histogram of mitochondria–lysosome contact site tethering duration in soma versus axons of peripheral sensory neurons. (Soma: n = 47 events from 10 neurons; Axon: n = 53 events from 13 neurons). Mean ± SEM.

We further analyzed whether defective mitochondria–lysosome contact untethering events were indeed mediated by disrupted Rab7 GTP hydrolysis. The mitochondrial TBC1D15 Rab7-GAP (GTPase activating protein) (19–22) promotes contact untethering by driving Rab7 GTP hydrolysis at mitochondria–lysosome contact sites (12, 13). We thus asked whether TBC1D15 expression was sufficient to rescue contact site dynamics in Rab7(V162M) neurons. Mitochondria–lysosome contacts formed in Rab7(V162M) neurons expressing TBC1D15 (*SI Appendix*, Fig. S9 *A–D*). However, contact sites in the axons of Rab7(V162M) neurons expressing TBC1D15 untethered by 160 s (yellow arrow; Fig. 2*E*). Moreover, detailed quantification of mitochondria–lysosome contact site dynamics demonstrated that TBC1D15 expression was sufficient to rescue both the percentage of lysosomes forming contacts in axons of Rab7(V162M) neurons (**$P < 0.01$; Fig. 2*G*), as well as significantly decrease the tethering duration of axonal mitochondria–lysosome contacts in Rab7(V162M) neurons (**$P < 0.01$; Fig. 2*I*). Indeed, additional analysis comparing mitochondria–lysosome contact site dynamics between soma and axon, demonstrated that Rab7(V162M) neurons showed significantly prolonged contact tethering in axons compared to the soma (*$P < 0.05$; *SI Appendix*, Fig. S10 *A–C*). In contrast, expression of TBC1D15 in Rab7(V162M) neurons reversed this, leading to decreased contact tethering durations in axons (*$P < 0.05$; *SI Appendix*, Fig. S10 *D–F*). In summary, prolonged mitochondria–lysosome contact tethering dynamics in the axons of Charcot–Marie–Tooth mutant Rab7(V162M) peripheral sensory neurons are mediated by disruption of Rab7 GTP hydrolysis.

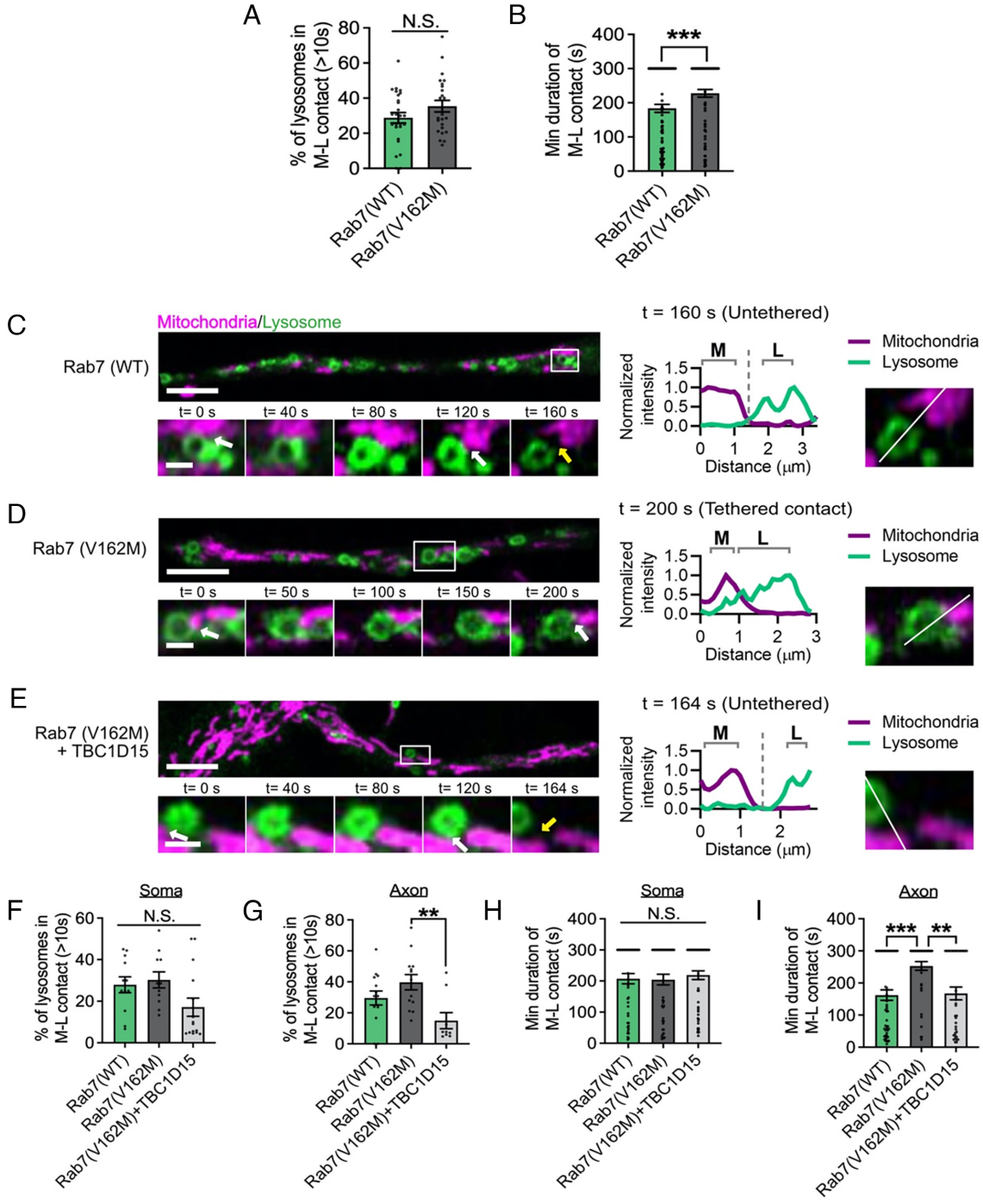

Fig. 2. Misregulation of mitochondria–lysosome contacts by Charcot–Marie–Tooth Type 2B mutant Rab7 in peripheral sensory neuron axons mediated by defective Rab7 GTP hydrolysis. (*A*) Quantification of percentage of lysosomes forming mitochondria–lysosome contact sites in Rab7(WT) versus Charcot–Marie–Tooth type 2B mutant Rab7(V162M) peripheral sensory neurons. [Rab7(WT): n = 14 neurons; Rab7(V162M): n = 14 neurons] [Mitochondria: MitoTracker Red; Lysosome: mNeonGreen-Rab7(WT) or (V162M)]. (*B*) Prolonged mitochondria–lysosome contact site tethering duration in mutant Rab7(V162M) peripheral sensory neurons compared to Rab7(WT). [Rab7(WT): n = 100 events from 13 neurons; Rab7(V162M): n = 88 events from 13 neurons]. (*C*) Confocal live microscopy time-lapse images and corresponding linescan of untethered mitochondria–lysosome contact (yellow arrow; t = 160 s) in the axon of Rab7(WT) peripheral sensory neurons. (Scale bar: 5 μm [*Top*], 1 μm [*Bottom*].) (*D*) Confocal live microscopy time-lapse images and corresponding linescan of prolonged tethered mitochondria–lysosome contact (white arrow; t = 200 s) in the axon of mutant Rab7(V162M) peripheral sensory neurons. (Scale bar: 5 μm [*Top*], 1 μm [*Bottom*].) (*E*) Confocal live microscopy time-lapse images and corresponding linescan of untethered mitochondria–lysosome contact (yellow arrow; t = 164 s) in the axon of Rab7(V162M) peripheral sensory neurons expressing Rab7-GAP (TBC1D15). (Scale bar: 5 μm [*Top*], 1 μm [*Bottom*].) (*F*) Quantification of percentage of lysosomes forming mitochondria–lysosome contact sites in the soma of Rab7(WT), mutant Rab7(V162M), and mutant Rab7(V162M) + TBC1D15 peripheral sensory neurons. [Rab7(WT): n = 12 neurons; Rab7(V162M): n = 11 neurons; Rab7(V162M)+TBC1D15: n = 15 neurons]. (*G*) Quantification of percentage of lysosomes forming mitochondria–lysosome contact sites in the axon of Rab7(WT), mutant Rab7(V162M), and mutant Rab7(V162M) + TBC1D15 peripheral sensory neurons. [Rab7(WT): n = 14 neurons; Rab7(V162M): n = 13 neurons; Rab7(V162M)+TBC1D15: n = 9 neurons]. (*H*) Quantification of mitochondria–lysosome contact site tethering duration in the soma of Rab7(WT), mutant Rab7(V162M), and mutant Rab7(V162M) + TBC1D15 peripheral sensory neurons. [Rab7(WT): n = 47 events from 10 neurons; Rab7(V162M): n = 46 events from 12 neurons; Rab7(V162M)+TBC1D15: n = 60 events from 14 neurons]. (*I*) Quantification of mitochondria–lysosome contact site tethering duration in the axon of Rab7(WT), mutant Rab7(V162M), and mutant Rab7(V162M) + TBC1D15 peripheral sensory neurons [Rab7(WT): n = 53 events from 13 neurons; Rab7(V162M): n = 42 events from 10 neurons; Rab7(V162M)+TBC1D15: n = 37 events from 10 neurons]. Mean ± SEM; $^{**}P < 0.01$; $^{***}P < 0.001$; NS, not significant.

Generation of Charcot–Marie–Tooth Type 2B Disease Mutant Rab7^{V162M} Knock-In Mouse Model. We then investigated whether mitochondria–lysosome contact dynamics were further disrupted in peripheral sensory neurons from an in vivo model of Charcot–Marie–Tooth type 2B. To address this, we generated a new mouse model of Charcot–Marie–Tooth type 2B expressing heterozygous CRISPR knock-in Charcot–Marie–Tooth disease Rab7(V162M) mutant (Fig. 3*A*; Rab7^{V162M}), consistent with the autosomal dominant form of the disease. Peripheral sensory neurons were cultured from Rab7^{WT} and Rab7^{V162M} mice, and subsequently imaged using live microscopy for mitochondria and lysosomes (Fig. 3 *B* and *C*). We first examined whether Rab7^{V162M} mice exhibited changes in lysosomal size, consistent with an established role for Rab7 in regulating late endosomal/lysosomal morphology (18). Indeed, lysosomes were significantly larger in the soma of peripheral sensory neurons from mutant Rab7^{V162M} mice compared to Rab7^{WT} mice (**P < 0.01; Fig. 3 *D*–*F* and *SI Appendix*, Fig. S11*A*). Consistent with these findings, lysosomal size was also preferentially increased in the soma of peripheral sensory neurons expressing Charcot–Marie–Tooth mutant Rab7(V162M) compared to Rab7(WT) (*SI Appendix*, Fig. S11 *B* and *C*). Of note, expression of Rab7(WT) alone increased lysosomal size compared to LysoTracker (μm: LysoTracker: 0.61 ± 0.02; Rab7 WT: 1.39 ± 0.07; ***P < 0.001), further demonstrating an established role for Rab7 in regulating lysosomal morphology. Thus, consistent with a role for Rab7 in regulating late endosomal/lysosomal dynamics (18), we find that lysosomes are disrupted in peripheral sensory neurons from Charcot–Marie–Tooth mutant Rab7^{V162M} mice.

Prolonged Mitochondria–Lysosome Contact Tethering in Peripheral Sensory Neurons from Charcot–Marie–Tooth Type 2B Disease Mutant Rab7^{V162M} Mice. We then analyzed whether mitochondria–lysosome contact dynamics were misregulated in the soma or axons of Rab7^{V162M} mice sensory neurons. Mitochondria–lysosome contact sites also dynamically formed in peripheral sensory neurons from Rab7^{WT} and Rab7^{V162M} mice (Fig. 4 *A*–*F*). Mitochondria–lysosome contacts had undergone untethering events in Rab7^{WT} neurons by ~160 s (yellow arrow; Fig. 4 *A*–*C*). In contrast, contacts remained dynamically tethered together in Rab7^{V162M} neurons at this timepoint (white arrows; Fig. 4 *D*–*F*). Importantly, while the percentage of lysosomes forming contacts was not disrupted in either the soma or axons of Rab7^{V162M} neurons (Fig. 4 *G* and *H*), mitochondria–lysosome contact site duration was preferentially increased in the axons of peripheral neurons from Charcot–Marie–Tooth mutant Rab7^{V162M} mice (**P < 0.01; Fig. 4*J*) but not in the soma (Fig. 4*I*). Together, these findings are consistent with our observations in sensory neurons expressing mutant Rab7(V162M) (Fig. 2 *F*–*I*) and further support a role for preferential defective mitochondria–lysosome contact site untethering in the axons of Charcot–Marie–Tooth mutant Rab7 peripheral sensory neurons.

To further determine whether decreased mitochondria–lysosome contact untethering events were mediated by defective Rab7 GTP hydrolysis, we expressed TBC1D15 (Rab7-GAP) in peripheral sensory neurons from Charcot–Marie–Tooth mutant Rab7^{V162M} mice, and investigated its ability to rescue changes in mitochondria–lysosome contact site dynamics. Importantly, TBC1D15 significantly rescued the prolonged axonal mitochondria–lysosome contact duration (Fig. 4*J*) observed in peripheral neurons from Charcot–Marie–Tooth mutant Rab7^{V162M} mice, but did not alter mitochondria–lysosome contact duration in the soma which was not changed in peripheral neurons from mutant Rab7^{V162M} mice (Fig. 4*I*), or the percentage of lysosomes in contact with mitochondria in the soma (Fig. 4*G*) or axons (Fig. 4*H*) which were also not changed. In summary, we further show that mitochondria–lysosome contact untethering events which are mediated by Rab7 GTP hydrolysis are also misregulated in peripheral sensory neurons from Charcot–Marie–Tooth mutant Rab7^{V162M} mice.

Defective Mitochondrial Network Dynamics in Charcot–Marie–Tooth Type 2B Disease Mutant Rab7^{V162M} Mice. Mitochondria–lysosome contact sites play a critical role in modulating mitochondrial dynamics including regulating mitochondrial motility (12, 16, 17), but whether defects in this pathway result in disrupted mitochondrial dynamics in peripheral sensory neurons from Charcot–Marie–Tooth mutant Rab7^{V162M} mice was not previously known. Detailed analysis of mitochondrial dynamics from live confocal microscopy time-lapse movies in peripheral sensory neurons demonstrated that peripheral sensory neurons from Rab7^{V162M} mice showed increased mitochondrial density (*P < 0.05; Fig. 5 *A*, *C* and *D*) and significantly decreased mitochondrial motility (*P < 0.05; Fig. 5*B*). In addition, the decrease in mitochondrial motility observed in peripheral sensory neurons from mutant Rab7^{V162M} mice (Fig. 5 *E* and *F*), was also found in neurons expressing Rab7(V162M) (*SI Appendix*, Fig. S12 *A*–*C*). To determine whether defective mitochondrial motility occurred downstream of defects in mitochondria–lysosome contact untethering, we investigated whether expressing TBC1D15 (Rab7-GAP) in peripheral sensory neurons from Charcot–Marie–Tooth mutant Rab7^{V162M} mice was able to rescue changes in mitochondrial motility. Interestingly, while TBC1D15 did not alter mitochondrial motility in the soma (Fig. 5*G*), expression of TBC1D15 was able to significantly increase mitochondrial motility in axons of peripheral sensory neurons from Charcot–Marie–Tooth mutant Rab7^{V162M} mice (**P < 0.01; Fig. 5*H*). Together, these findings highlight a pathway for Rab7 GTP hydrolysis in driving mitochondria–lysosome contact site untethering to modulate downstream mitochondrial motility, which is directly disrupted in Charcot–Marie–Tooth disease mutant Rab7 peripheral neurons.

To further investigate defects in mitochondrial morphology in Charcot–Marie–Tooth type 2B mutant Rab7^{V162M} mice, we conducted electron microscopy (EM) analysis of mitochondria in sciatic nerves taken from Rab7^{WT} and Rab7^{V162M} mice (Fig. 6*A*). Using EM analysis as previously described (23, 24), mitochondrial area, perimeter, and roundness were not disrupted in Rab7^{V162M} mice (*SI Appendix*, Fig. S13 *A*–*C*). However, mitochondrial morphology including circularity, interconnectivity, aspect ratio and form factor were significantly disrupted in mitochondria in sciatic nerves from Charcot–Marie–Tooth mutant Rab7^{V162M} mice, as compared to Rab7^{WT} mice (Fig. 6 *B*–*E*). Specifically, mitochondria in the axons of sciatic nerves from mutant Rab7^{V162M} mice demonstrated significantly decreased circularity (*P < 0.05; Fig. 6*B*), interconnectivity (*P < 0.05; Fig. 6*C*), and aspect ratio (***P < 0.001; Fig. 6*D*), as compared to Rab7^{WT} mice. The lower score in interconnectivity and aspect ratio indicates a fragmented mitochondrial morphology in the sciatic nerves of mutant Rab7^{V162M} mice. Furthermore, mitochondrial branching (form factor) was significantly increased in mitochondria in sciatic nerves from mutant Rab7^{V162M} mice compared to Rab7^{WT} mice (*P < 0.05; Fig. 6*E*). The observed altered mitochondria morphology with fragmented mitochondria in the axon of the sciatic nerve could be particularly relevant from the point of view of axonal degeneration in mutant Rab7 Charcot–Marie–Tooth type 2B disease and further demonstrate mitochondrial dysfunction in Charcot–Marie–Tooth mutant Rab7^{V162M} mice.

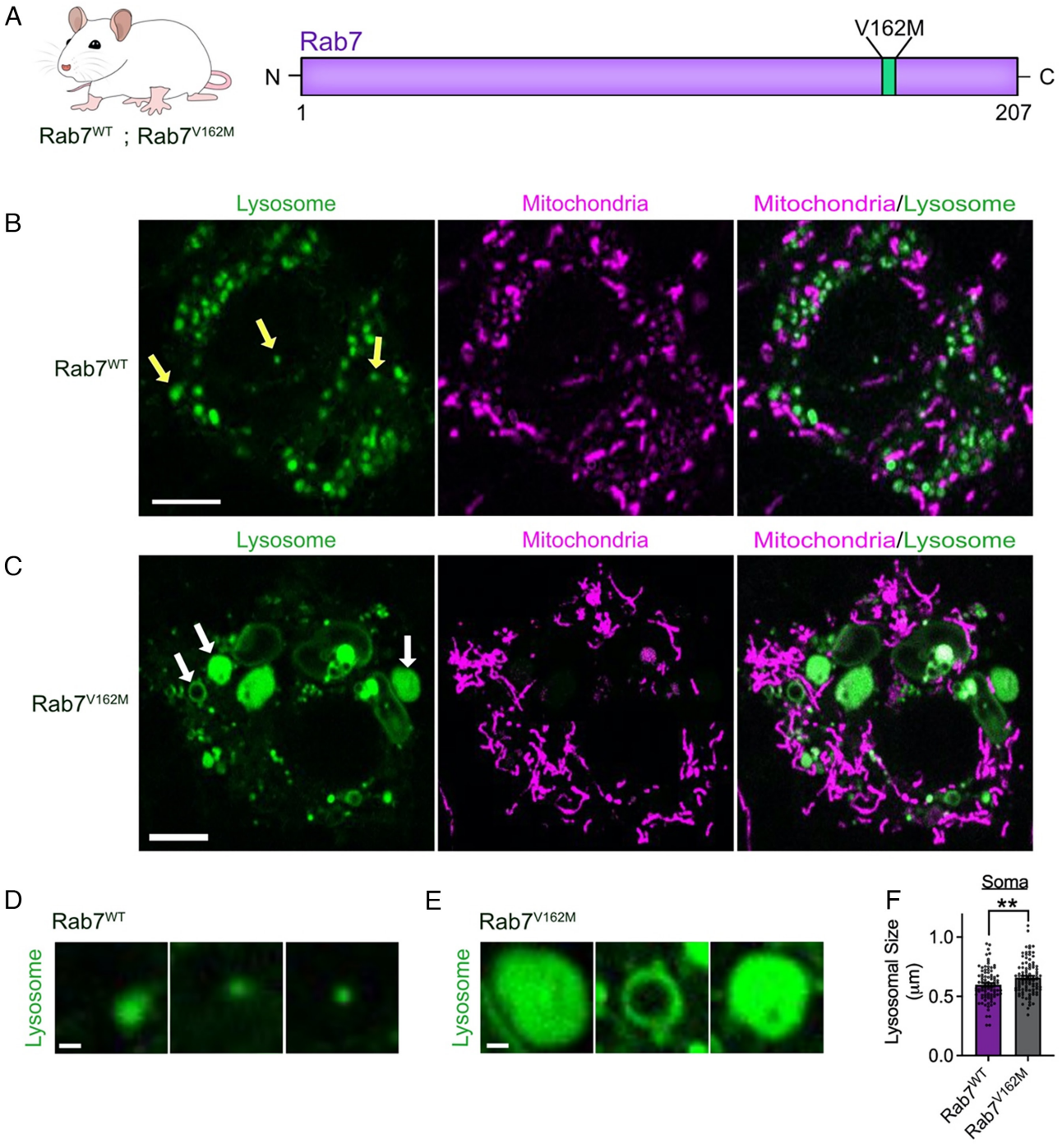

Fig. 3. Generation of Charcot–Marie–Tooth Type 2B disease mutant Rab7^{V162M} knock-in mouse model. (*A*) Schematic of Charcot–Marie–Tooth type 2B disease mutation in heterozygous Rab7^{V162M} knock-in mouse model. (*B*) Confocal live microscopy image of mitochondria (MitoTracker Red) and lysosomes (LysoTracker Far Red) in peripheral sensory neurons from Rab7^{WT} mice. (Scale bar: 5 μm.) (*C*) Confocal live microscopy image of mitochondria (MitoTracker Red) and lysosomes (LysoTracker Far Red) in peripheral sensory neurons from mutant Rab7^{V162M} mice, demonstrating enlarged lysosomes (white arrows). (Scale bar: 5 μm.) (*D* and *E*) Confocal live microscopy image of lysosomes in peripheral sensory neurons from Rab7^{WT} mice (*D*) or mutant Rab7^{V162M} mice (*E*) corresponding to arrows in Fig. 3 *B* and *C*. (Scale bar: 0.5 μm [*D*], 0.5 μm [*E*].) (*F*) Quantification of enlarged lysosomes in the soma of peripheral sensory neurons from mutant Rab7^{V162M} mice. (Rab7^{WT}: n = 90 lysosomes from 18 neurons; Rab7^{V162M}: n = 95 lysosomes from 19 neurons). Mean ± SEM; $^{**}P < 0.01$.

Charcot–Marie–Tooth Type 2B Disease Mutant Rab7^{V162M} Mice Exhibit Sensory Behavioral Abnormalities. Finally, we investigated whether the defective mitochondrial and lysosomal dynamics we observed in peripheral sensory neurons from Charcot–Marie–Tooth mutant Rab7^{V162M} mice might ultimately result in sensory behavior abnormalities in these mice. Of note, Charcot–Marie–Tooth type 2B patients with Rab7^{V162M} mutation show preferential sensory phenotypes rather than motor phenotypes (3, 7). Thus, we further interrogated whether Rab7^{V162M} mice preferentially demonstrated sensory abnormalities over motor deficits. Rab7^{V162M} mice were analyzed for sensory abnormalities, in particular mechanical allodynia, by quantifying the withdrawal threshold of the hindpaw in response to stimulation with flexible von Frey filaments applied in order of ascending force as previously described (25–27). Importantly, Rab7^{V162M} mice exhibited a significantly reduced withdrawal threshold compared to aged-matched Rab7^{WT} mice, indicating the development of mechanical allodynia ($^{***}P < 0.001$; Fig. 7*A*), thus demonstrating sensory behavior abnormalities in mutant Rab7^{V162M}

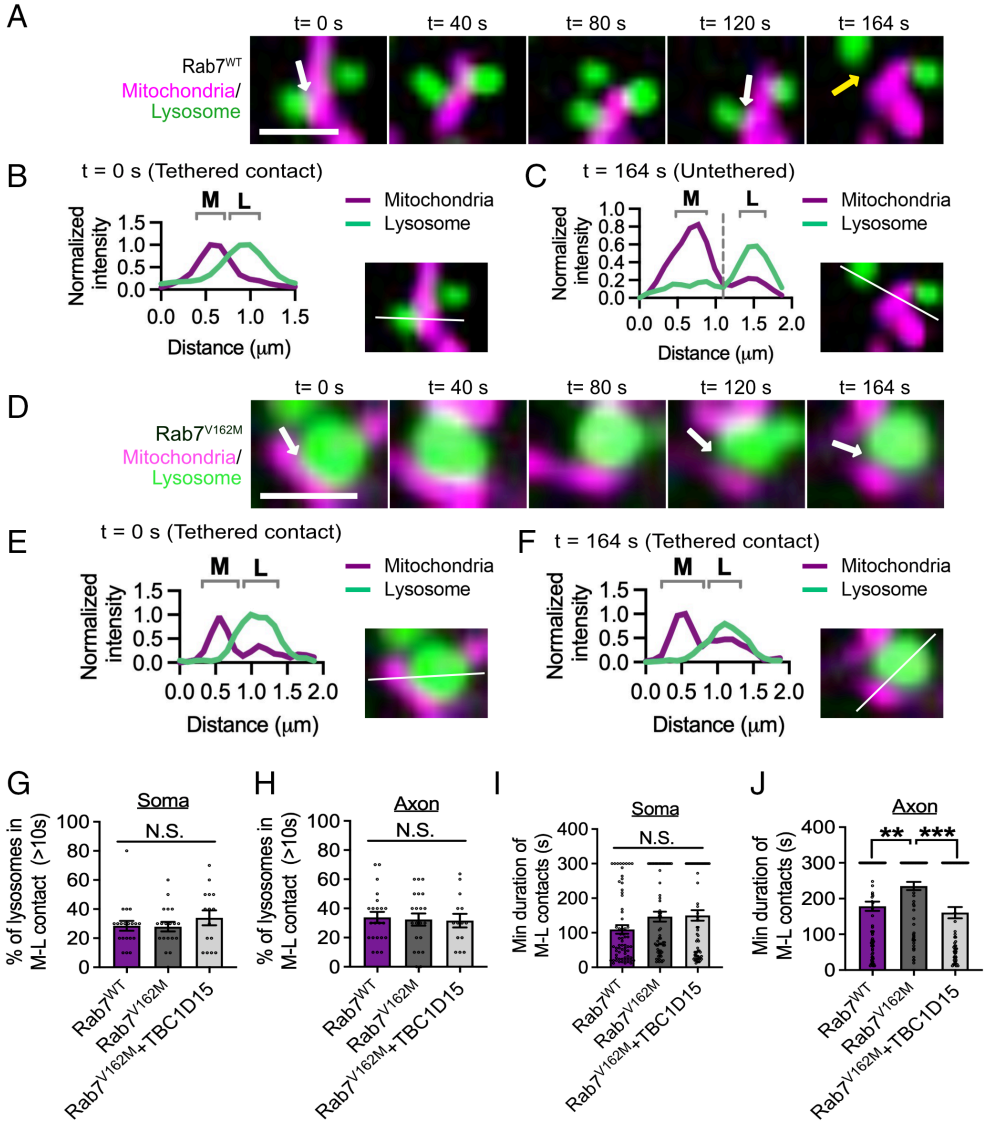

Fig. 4. Prolonged mitochondria–lysosome contact tethering in peripheral sensory neurons from Charcot–Marie–Tooth Type 2B disease mutant Rab7^{V162M} mice. (*A*) Confocal live microscopy time-lapse images of mitochondria–lysosome contact site untethering in peripheral sensory neurons from Rab7^{WT} mice (white arrow, contact tethered; yellow arrow, untethered contact) (Mitochondria: MitoTracker Red; Lysosome: LysoTracker Far Red). (Scale bar: 1 μm.) (*B*) Linescan of mitochondria and lysosome tethered at contact (t = 0 s), corresponding to Fig. 4*A*. (*C*) Linescan of mitochondria and lysosome contact untethered (t = 164 s), corresponding to Fig. 4*A*. (*D*) Confocal live microscopy time-lapse images of prolonged mitochondria–lysosome contact site tethering in peripheral sensory neurons from mutant Rab7^{V162M} mice (white arrow, contact tethered) (Mitochondria: MitoTracker Red; Lysosome: LysoTracker Far Red). (Scale bar: 1 μm.) (*E*) Linescan of mitochondria and lysosome tethered at contact (t = 0 s), corresponding to Fig. 4*D*. (*F*) Linescan of mitochondria and lysosome still tethered at contact (t = 164 s), corresponding to Fig. 4*D*. (*G* and *H*) Quantification of percentage of lysosomes forming mitochondria–lysosome contact sites in soma (*G*) and axons (*H*) in peripheral sensory neurons from Rab7^{WT} mice versus mutant Rab7^{V162M} mice versus neurons from mutant Rab7^{V162M} mice expressing TBC1D15. (Soma: Rab7^{WT}: n = 20 neurons; Rab7^{V162M}: n = 19 neurons; Rab7^{V162M}+TBC1D15: n = 15 neurons; Axon: Rab7^{WT}: n = 22 neurons; Rab7^{V162M}: n = 21 neurons; Rab7^{V162M}+TBC1D15: n = 14 neurons). (*I* and *J*) Mitochondria–lysosome contact site tethering duration in axons is prolonged in peripheral sensory neurons from mutant Rab7^{V162M} mice and rescued by TBC1D15 expression (*I*), but not altered in the soma (*J*). (Soma: Rab7^{WT}: n = 66 events from 17 neurons; Rab7^{V162M}: n = 62 events from 15 neurons; Rab7^{V162M}+TBC1D15: n = 64 events from 15 neurons; Axon: Rab7^{WT}: n = 84 events from 19 neurons; Rab7^{V162M}: n = 76 events from 18 neurons; Rab7^{V162M}+TBC1D15: n = 64 events from 14 neurons). Mean ± SEM; $^{**}P < 0.01$; $^{***}P < 0.001$; NS, not significant.

mice. We next investigated whether Rab7^{V162M} mice had motor deficits by performing rotarod tests. Rab7^{V162M} mice and age-matched Rab7^{WT} mutant mice were subjected to three days of habituation and two days of acceleration. Interestingly, motor behaviors of both Rab7^{WT} and Rab7^{V162M} mice were not different on any of the habituation or acceleration rotarod tests (Fig. 7*B*). Moreover, gait dynamics were also not disrupted in Charcot–Marie–Tooth mutant Rab7^{V162M} mice (*SI Appendix*, Fig. S14 *A–F*). Together, these findings are consistent with that of patients with Charcot–Marie–Tooth type 2B, which is clinically characterized by predominant sensory loss and evoked pain with lesser-to-absent motor deficits (2–7, 28). As some patients exhibit distal muscle weakness with distal leg muscles more affected than hand muscles (2–8, 28), we also examined whether there was distal weakness in hind limbs by conducting grip strength analysis and found no differences between mutant Rab7^{V162M} mice and age-matched Rab7^{WT} mice (*SI Appendix*, Fig. S14*G*). Overall, these findings demonstrate that Rab7^{V162M} mice preferentially exhibit sensory abnormalities.

Degeneration of peripheral sensory nerve terminals which extend to innervate the skin results in small fiber neuropathy and is reflected by a decreased intra-epidermal nerve fiber density observed in the skin of Charcot–Marie–Tooth type 2B patients (8). As such, we investigated whether mutant Rab7^{V162M} mice also exhibited small-fiber degeneration, by examining intra-epidermal nerve fiber density in skin samples from Rab7^{WT} and mutant Rab7^{V162M} mice subjected to confocal microscopy analysis. Of note, Charcot–Marie–Tooth mutant

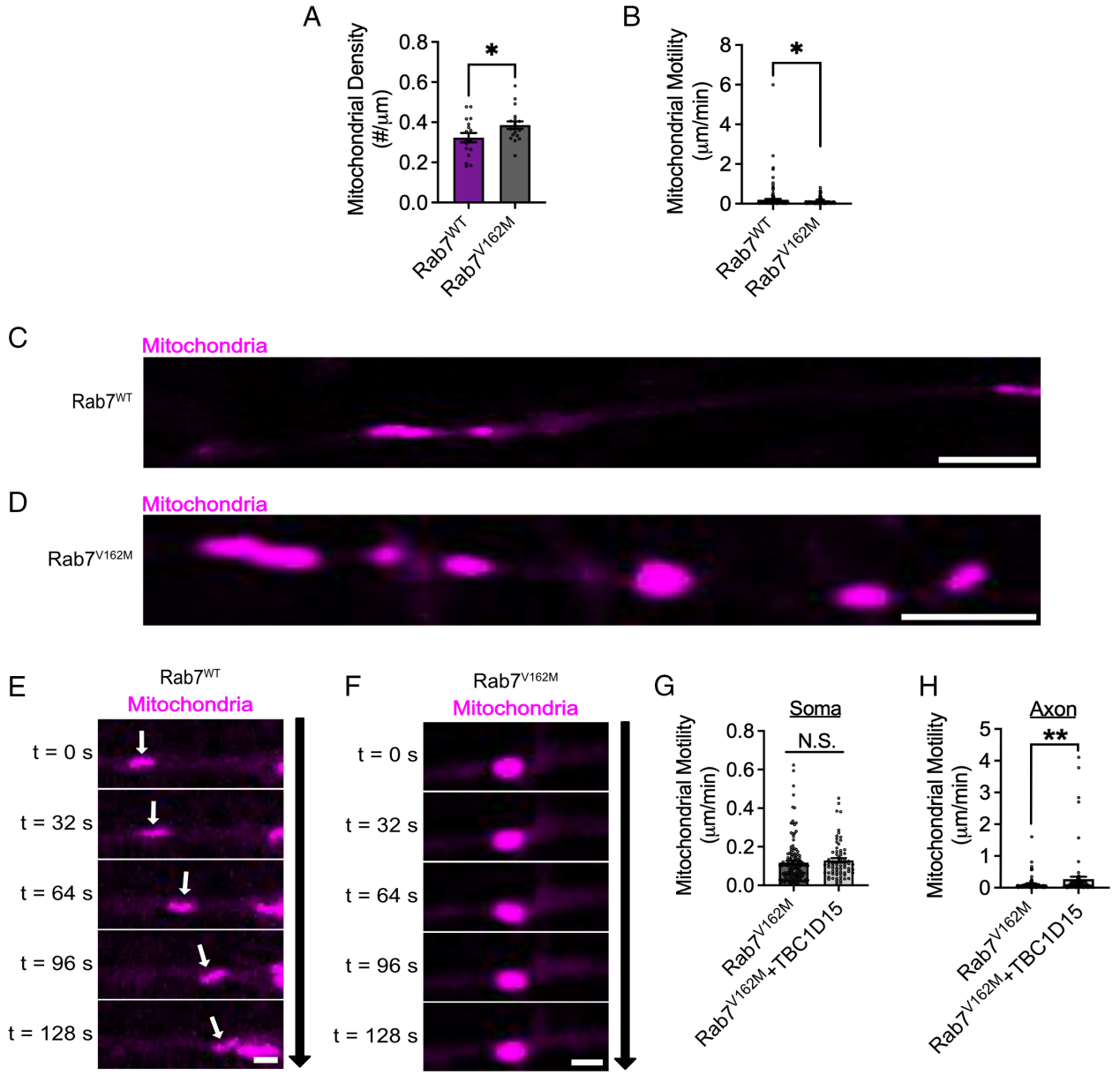

Fig. 5. Defective mitochondrial dynamics in peripheral sensory neurons from Charcot–Marie–Tooth Type 2B disease mutant Rab7^{V162M} mice. (*A*) Quantification of increased mitochondrial density in peripheral sensory neurons from mutant Rab7^{V162M} mice. (Rab7^{WT}: n = 17 neurons; Rab7^{V162M}: n = 17 neurons). (*B*) Quantification of disrupted mitochondrial motility in peripheral sensory neurons from Charcot–Marie–Tooth type 2B mutant Rab7^{V162M} mice, as compared to Rab7^{WT} mice. (Rab7^{WT}: n = 165 events from 18 neurons; Rab7^{V162M}: n = 190 events from 19 neurons). (*C* and *D*) Confocal live microscopy images of mitochondria in peripheral sensory neurons from Rab7^{WT} mice and mutant Rab7^{V162M} mice (Mitochondria: MitoTracker Red). (Scale bar: 2.5 µm [C]; 2.5 µm [D].) (*E* and *F*) Confocal live microscopy time-lapse images of motile mitochondria (white arrows) in peripheral sensory neurons from Rab7^{WT} mice, compared to stationary mitochondria in peripheral sensory neurons from mutant Rab7^{V162M} mice. (Scale bar: 1 µm [E]; 1 µm [F].) (*G* and *H*) Decreased mitochondrial motility in axons of peripheral sensory neurons from mutant Rab7^{V162M} mice is rescued by TBC1D15 expression (*H*), but not altered in the soma (*G*). (Soma: Rab7^{V162M}: n = 144 events from 29 neurons; Rab7^{V162M}+TBC1D15: n = 70 events from 14 neurons; Axon: Rab7^{V162M}: n = 145 events from 29 neurons; Rab7^{V162M}+TBC1D15: n = 85 events from 17 neurons). Mean ± SEM; *P < 0.05; **P < 0.01; NS, not significant.

Rab7^{V162M} mice displayed a dramatic reduction in intra-epidermal nerve fiber density (IENF density), expressed as the number of nerves crossing the epidermal–dermal junction as a function of length, as compared to Rab7^{WT} mice (*P < 0.05; Fig. 7 *C* and *D* and *SI Appendix*, Fig. S15*A*). Together, our study demonstrates preferential sensory behavior deficits and neuropathy in a mutant Rab7 mouse model of Charcot–Marie–Tooth type 2B disease.

Discussion

Mitochondria–lysosome contact sites play critical roles in mediating the bidirectional crosstalk between mitochondria and lysosomes (13, 14). Elucidating the role of these contact sites in neurons and their contribution to disease is key for shedding light on the role of mitochondria–lysosome contacts in neuronal homeostasis. Here, we used live super-resolution and confocal time-lapse microscopy to investigate mitochondria–lysosome contact formation and dynamics in peripheral sensory neurons. Both mitochondria and lysosomes were identified throughout both the soma and axons, and further formed dynamic mitochondria–lysosome contact sites in both neuronal compartments over time, with similar formation and tethering duration dynamics in peripheral sensory neurons. Our findings are consistent with the formation of mitochondria–lysosome contact sites in multiple cell types (12, 13, 29–34), including retinal ganglion cells and dopaminergic neurons (35, 36), suggesting that

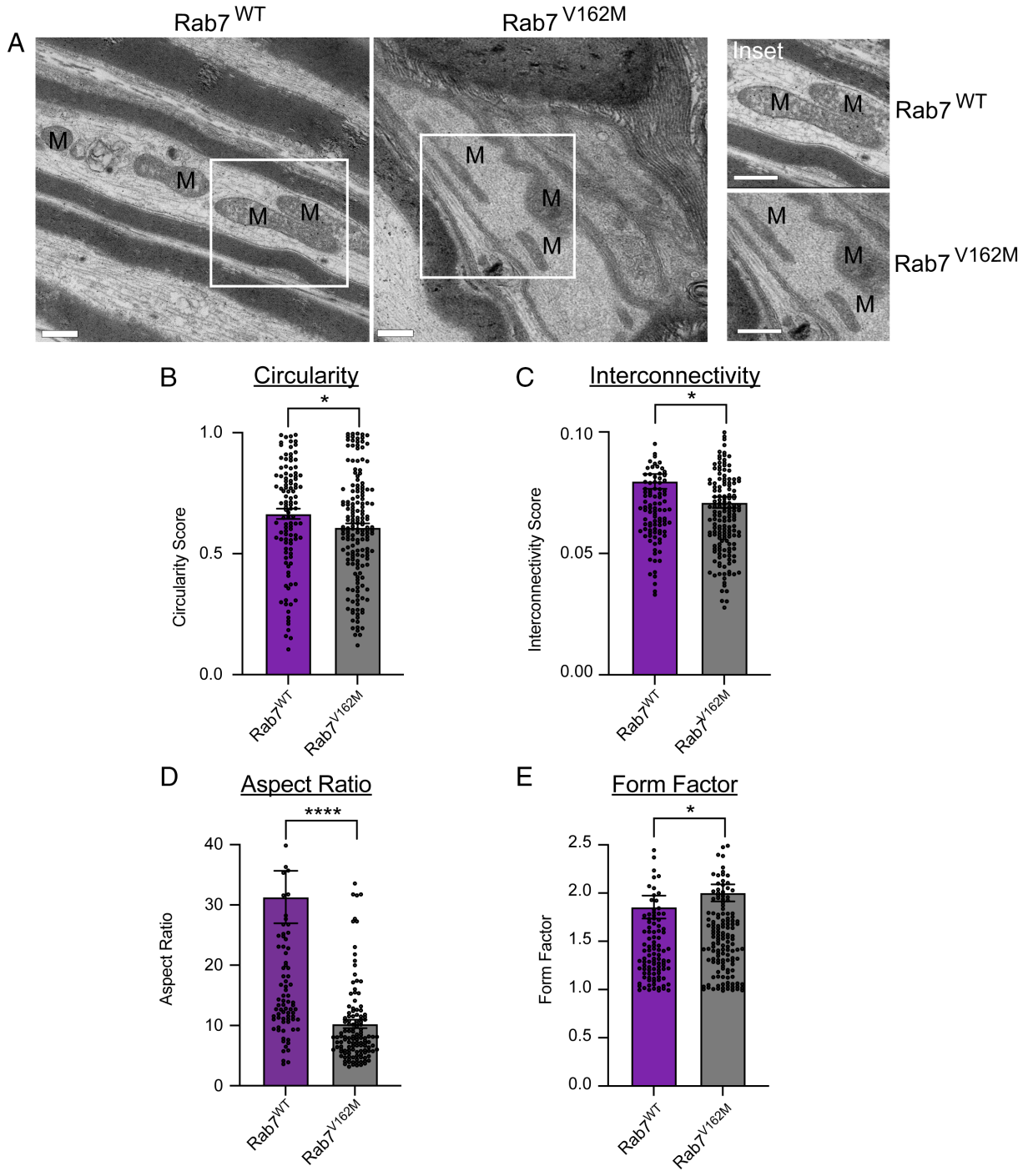

Fig. 6. Disrupted mitochondrial network in Charcot–Marie–Tooth Type 2B disease mutant Rab7^{V162M} mice. (*A*) Electron micrographs (EM) of sciatic nerves from Rab7^{WT} and Charcot–Marie–Tooth type 2B mutant Rab7^{V162M} mice. (Scale bar: 500 nm; M: mitochondria.) (*B*–*E*) Analysis from EM images of disrupted mitochondrial circularity, interconnectivity, aspect ratio, and form factor in sciatic nerves from mutant Rab7^{V162M} mice, as compared to Rab7^{WT} mice. (Rab7^{WT}: n = 115 mitochondria; Rab7^{V162M}: n = 168 mitochondria). Mean ± SEM; *$P < 0.05$, ****$P < 0.001$.

mitochondria–lysosome contacts may play key roles in mediating the homeostasis of multiple cellular and neuronal populations.

The small GTPase Rab7 is critical for regulating late endosomal/lysosomal dynamics (18), and Rab7 GTP hydrolysis has been shown to drive mitochondria–lysosome contact site untethering events, mediated by the mitochondrial TBC1D15 Rab7-GAP (12). Charcot–Marie–Tooth type 2B Rab7 mutants disrupt Rab7 GTP hydrolysis (9–11), pointing to a critical role for defective mitochondria–lysosome contact untethering in driving the etiology of Charcot–Marie–Tooth type 2B disease (16, 36), and the degeneration of peripheral sensory neurons. Indeed, while Charcot–Marie–Tooth type 2B mutant Rab7 misregulates mitochondria–lysosome contacts (16), whether this occurs in peripheral sensory neurons was not known. Here, we show that mitochondria–lysosome contact site untethering is disrupted in peripheral sensory neurons, resulting in prolonged contact tethering in Charcot–Marie–Tooth type 2B mutant Rab7 neurons. Interestingly, this defect preferentially occurred in axons but not the soma of these neurons, highlighting a potential mechanism contributing to the axonal degeneration observed in Charcot–Marie–Tooth type 2.

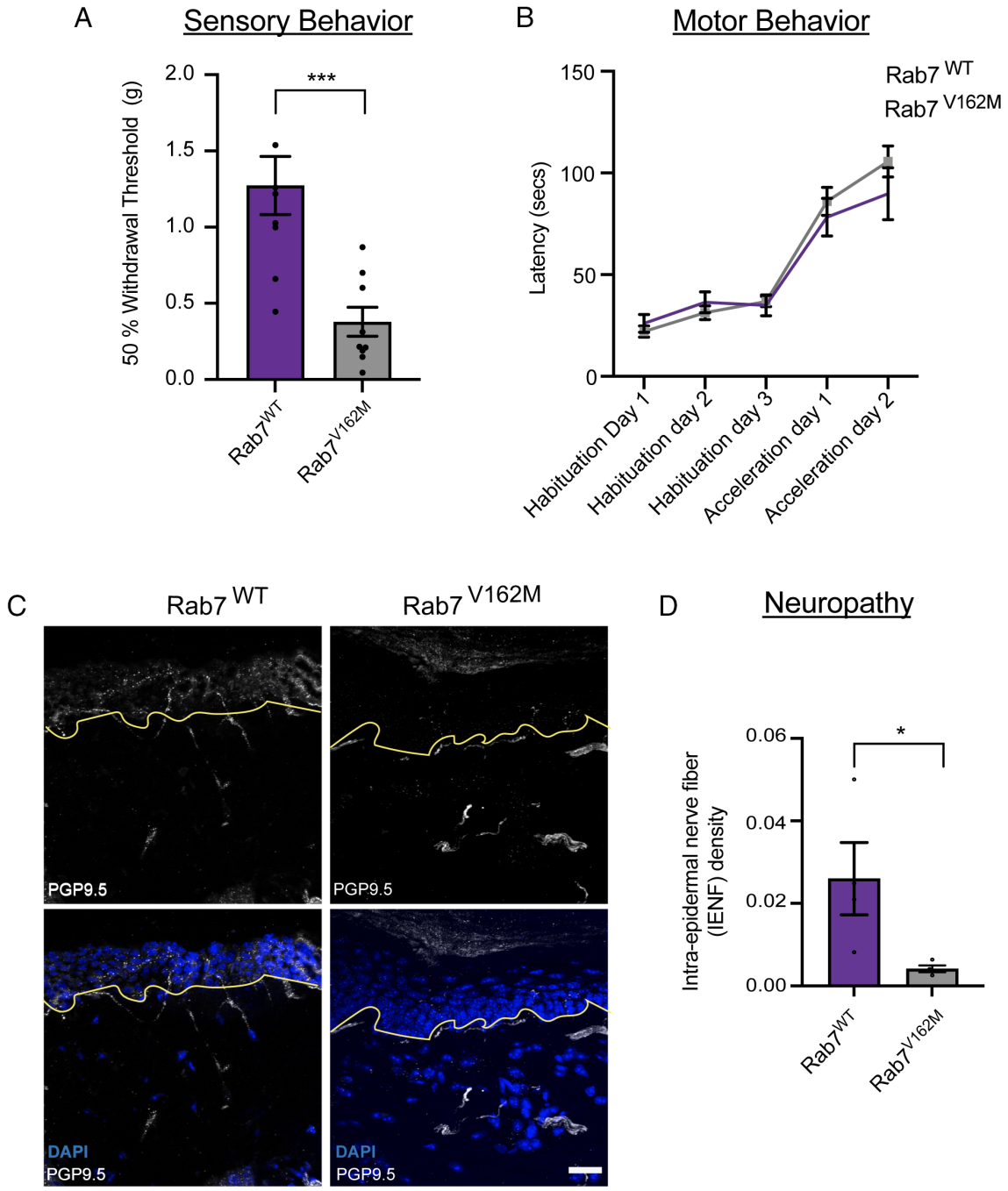

Fig. 7. Charcot–Marie–Tooth Type 2B disease mutant Rab7^{V162M} mice exhibit preferential sensory behavioral abnormalities. (*A*) Sensory behavioral deficit in Charcot–Marie–Tooth type 2B mutant Rab7^{V162M} mice, assessed by mechanical allodynia measured using the von Frey analysis. (Rab7^{WT}: n = 9 mice; Rab7^{V162M}: n = 9 mice). (*B*) Normal motor behavior in Charcot–Marie–Tooth type 2B mutant Rab7^{V162M} mice, assessed by rotarod test to measure motor deficits. (Rab7^{WT}: n = 18 mice; Rab7^{V162M}: n = 30 mice). (*C* and *D*) Defective skin innervations in Charcot–Marie–Tooth type 2B mutant Rab7^{V162M} mice, assessed by intra-epidermal nerve fiber (IENF) density. Confocal imaging analysis and quantification of IENF density skin from Rab7^{WT} and Rab7^{V162M} mice showing PGP9.5 (pseudo-colored in gray, top) and merged images with the nuclear marker DAPI (blue, bottom). The solid line demarcates the epidermal–dermal junction. (Scale bar: 50 μm.) (Rab7^{WT}: n = 4 mice; Rab7^{V162M}: n = 4 mice). Mean ± SEM; *P < 0.05, ***P < 0.001.

Importantly, defects in mitochondria–lysosome contact site dynamics could be rescued by Rab7 GAP (TBC1D15), further demonstrating a role for Rab7 GTP hydrolysis at mitochondria–lysosome contacts in driving untethering events, which are disrupted in Charcot–Marie–Tooth type 2B mutant Rab7 neurons.

Properly regulated mitochondrial dynamics are essential for neurons, and mitochondria–lysosome contacts have been found to be key regulators of mitochondrial dynamics (12, 13, 16, 17), including both mitochondrial fission and inter-mitochondrial untethering which are regulated by Drp1 GTP hydrolysis (16, 37). Interestingly, Drp1 GTP hydrolysis was recently shown to be coregulated with Rab7 GTP hydrolysis via an oligomeric complex of Mid51 and Fis1 on the mitochondrial membrane, allowing for the respective bidirectional regulation of both mitochondrial and lysosomal dynamics at mitochondria–lysosome contact sites (17). Here, we showed that Charcot–Marie–Tooth type 2B mutant Rab7 peripheral sensory neurons exhibit defects in mitochondrial dynamics which could be rescued by targeting Rab7 GTP hydrolysis machinery, further highlighting a role for mitochondrial dysfunction in Charcot–Marie–Tooth disease. Defective mitochondrial dynamics

have been implicated in multiple genetic forms of Charcot–Marie–Tooth type 2 characterized by the axonal degeneration of peripheral neurons (38), including Mfn2-associated Charcot–Marie–Tooth type 2A disease (39–42), TRPV4-associated Charcot–Marie–Tooth type 2C disease (16, 43–46), and GDAP1-associated Charcot–Marie–Tooth type 2K disease (47, 48). Our findings further underscore mitochondrial defects as a key contributor to Rab7-associated Charcot–Marie–Tooth type 2B disease (16, 36, 49) and demonstrate the importance of properly regulated mitochondrial dynamics in peripheral neurons.

Mitochondrial dynamics reflect ongoing changes in inter-mitochondrial networks as well as mitochondrial shape, size, connectivity, trafficking, and activity (50). Mitochondrial morphology, which can range from an interconnected reticulum to fragmented puncta, is determined by the balance between the opposing forces of fusion and fission (51). Here, we show that mitochondria in the axons of sciatic nerves in Charcot–Marie–Tooth type 2B mutant Rab7 knock-in mice further displayed fragmented morphology. Defects in mitochondrial morphology and dynamics can compromise mitochondrial functions, and ultimately affect neuronal survival and function (52–54). Thus, altered mitochondrial morphology with fragmented mitochondria may be particularly relevant from the perspective of axonal degeneration.

Peripheral sensory neurons are predominantly affected in Charcot–Marie–Tooth type 2B disease (3–7). Importantly, the generation of new Charcot–Marie–Tooth type 2 in vivo models has provided key insights into both the cellular mechanisms and etiology of peripheral neuropathies (49, 55–62). Here, we generated a Charcot–Marie–Tooth type 2B mutant Rab7 knock-in mouse model, which preferentially demonstrated sensory abnormalities. In particular, we found that mutant Rab7^{V162M} mice developed a type of pain hypersensitivity called mechanical allodynia. Consistent with our findings, pain has been reported in Charcot–Marie–Tooth type 2B patients (6, 8) in addition to distal sensory deficits (2–8).

Moreover, reduction in intra-epidermal nerve fiber (IENF) density, generally associated with neuropathic pain, has also been observed in the skin of Charcot–Marie–Tooth type 2B patients (8). Consistent with these clinical observations, our study demonstrates that mutant Rab7^{V162M} mice displayed a dramatic reduction in intra-epidermal nerve fiber density consistent with small fiber neuropathy. This is the result of axonal degeneration of nerve terminals, which are the long axon of DRG sensory neurons carrying pain, nociceptors, extending to innervate the skin. In particular, DRG neurons are especially dependent on efficient mitochondrial trafficking dynamics because of their unique morphology and long axons (63–66). Importantly, we observed significantly disrupted mitochondrial motility in sensory peripheral neurons of mutant Rab7^{V162M} mice. In addition, sensory peripheral neurons from mutant Rab7^{V162M} mice exhibited lysosomal defects, consistent with misregulation of Rab7's role in the late endosomal/ lysosomal pathway in Charcot–Marie–Tooth type 2B (11, 18, 36, 67–70). Finally, sensory peripheral neurons from mutant Rab7^{V162M} mice exhibited defective axonal mitochondria–lysosome contact untethering dynamics, consistent with a key role for mitochondria–lysosome contacts mediated by Rab7 GTP hydrolysis in regulating mitochondrial dynamics (12, 16, 17, 35). Thus, while our findings do not directly demonstrate that sensory neuropathy is caused by mitochondria–lysosome contact site defects in Rab7 mutant Charcot–Marie–Tooth type 2B disease, we found that mitochondria–lysosome contact sites dynamically form in sensory neurons and play an important role in modulating mitochondrial dynamics, which is disrupted in disease mutant Rab7 neurons. Importantly, future studies investigating the mechanisms underlying axonal neurodegeneration in sensory peripheral neurons in Charcot–Marie–Tooth type 2B will help to shed additional light on the role of this pathway in driving neurodegeneration.

In summary, our results point to an important role for mitochondria–lysosome contact sites in axons of peripheral sensory neurons, which are primarily affected in Charcot–Marie–Tooth type 2B. Contact sites between mitochondria and lysosomes are critical for regulating the homeostasis of both organelles (13, 14). Moreover, defects in this important pathway have been recently linked to the pathogenesis of multiple neurodegenerative diseases including Parkinson's disease and lysosomal storage disorders (14, 16, 17, 35, 47, 71–75). Together, this work provides insights into mitochondria–lysosome contact site regulation in peripheral neurons and has important consequences for the fields of inter-organelle contact site biology, peripheral neuropathy, and neurodegenerative diseases.

Materials and Methods

Detailed materials and methods are included in *SI Appendix*, Materials and Methods.

Culture of DRG Sensory Peripheral Neurons. DRG neurons from wildtype mice were acutely dissociated and digested with collagenase IV (1 μg/mL) and papain (30 U/mL) (Worthington Biochemical Corp). Neurons were plated on laminin (20 μg/mL) and poly-L-lysine (20 μg/mL)-coated glass coverslips and cultured at 37 °C with 5% CO_2 for 48 h in adult neurogenic medium: F12 with L-glutamine, 0.5% fetal bovine serum, 1× N2 (Life Technologies), penicillin (100 μg/mL), and streptomycin (100 U/mL).

Confocal Live Microscopy. Confocal time-lapse live images were acquired on a Nikon A1R laser scanning confocal microscope with GaAsp detectors using a Plan Apo λ 100× 1.45 NA oil immersion objective (Nikon) using NIS-Elements (Nikon). Live cells were imaged in a temperature-controlled chamber (37 °C) at 5% CO_2.

Graphing and Figure Assembly. Statistics and graphing were performed using Prism 7 (GraphPad) software. All statistical tests were justified as appropriate and were analyzed from N ≥ 3 independent experiments (biological replicates) per condition. Line scans were generated using ImageJ (NIH) and normalized per protein. All videos and images were assembled using ImageJ (NIH). All final figures were assembled in Affinity Designer (Affinity) or Illustrator (Adobe).

Data, Materials, and Software Availability. All study data are included in the article and/or *SI Appendix*.

ACKNOWLEDGMENTS. We thank Cavan Pellegrino for assistance in image analysis. We would also like to thank the Behavioral Phenotyping Core for their assistance in performing the behavioral experiments. Nikon confocal live imaging was performed at the Northwestern University Center for Advanced Microscopy generously supported by National Cancer Institute CCSG P30 CA060553 awarded to the Robert H. Lurie Comprehensive Cancer Center. We also thank the Genome Engineering Technologies service at The Jackson Laboratory (supported by NCI P30 CA034196). This work was supported by NIH grants to Y.C.W. (NINDS R00 NS109252), T.B.B. (NINDS Diversity Research Supplement 3R00NS109252-04S2), R.W.B. (NINDS R24 NS098523 and R37 NS054154), and D.M.M. (R01 NS104295-01, NIH HEAL initiative supplement R01 NS104295-01 and R01 AR077691-01).

Author affiliations: [a]Department of Neurology, Northwestern University Feinberg School of Medicine, Chicago, IL 60611; [b]The Jackson Laboratory, Bar Harbor, ME 04609; [c]Simpson Querrey Center for Neurogenetics, Northwestern University Feinberg School of Medicine, Chicago, IL 60611; and [d]Department of Pharmacology, Northwestern University Feinberg School of Medicine, Chicago, IL 60611

Author contributions: Y.C.W., N.D.J., D.K., R.W.B., and D.M.M. designed research; Y.C.W., N.D.J., T.B.B., G.C.S., H.E.B., D.R., A.L.D.T., and D.M.M. performed research; Y.C.W., N.D.J., T.B.B., G.C.S., H.E.B., A.L.D.T., R.W.B., and D.M.M. analyzed data; and Y.C.W., N.D.J., R.W.B., and D.M.M. wrote the paper.

The authors declare no competing interest.

1. A. M. Rossor, P. J. Tomaselli, M. M. Reilly, Recent advances in the genetic neuropathies. *Curr. Opin. Neurol.* **29**, 537–548 (2016).
2. D. Pareyson, P. Saveri, G. Piscosquito, Charcot-Marie-Tooth disease and related hereditary neuropathies: From gene function to associated phenotypes. *Curr. Mol. Med.* **14**, 1009–1033 (2014).
3. K. Verhoeven *et al.*, Mutations in the small GTP–ase late endosomal protein RAB7 cause Charcot-Marie-Tooth type 2B neuropathy. *Am. J. Hum. Genet.* **72**, 722–727 (2003).
4. H. Houlden *et al.*, A novel RAB7 mutation associated with ulcero-mutilating neuropathy. *Ann. Neurol.* **56**, 586–590 (2004).
5. F. Meggouh, H. M. Bienfait, M. A. Weterman, M. de Visser, F. Baas, Charcot–Marie–Tooth disease due to a de novo mutation of the RAB7 gene. *Neurology* **67**, 1476–1478 (2006).
6. X. Wang, C. Han, W. Liu, P. Wang, X. Zhang, A novel RAB7 mutation in a Chinese family with Charcot-Marie-Tooth type 2B disease. *Gene* **534**, 431–434 (2014).
7. F. Manganelli *et al.*, Autonomic nervous system involvement in a new CMT2B family. *J. Peripher. Nerv. Syst.* **17**, 361–364 (2012).
8. P. Saveri *et al.*, Charcot–Marie-Tooth Type 2B: A new phenotype associated with a novel RAB7A mutation and inhibited EGFR degradation. *Cells* **9**, 1028 (2020).
9. M. R. Spinosa *et al.*, Functional characterization of Rab7 mutant proteins associated with Charcot-Marie-Tooth type 2B disease. *J. Neurosci.* **28**, 1640–1648 (2008).
10. B. A. McCray, E. Skordalakes, J. P. Taylor, Disease mutations in Rab7 result in unregulated nucleotide exchange and inappropriate activation. *Hum. Mol. Genet.* **19**, 1033–1047 (2010).
11. K. Zhang *et al.*, Defective axonal transport of Rab7 GTPase results in dysregulated trophic signaling. *J. Neurosci.* **33**, 7451–7462 (2013).
12. Y. C. Wong, D. Ysselstein, D. Krainc, Mitochondria-lysosome contacts regulate mitochondrial fission via RAB7 GTP hydrolysis. *Nature* **554**, 382–386 (2018).
13. Y. C. Wong, S. Kim, W. Peng, D. Krainc, Regulation and function of mitochondria-lysosome membrane contact sites in cellular homeostasis. *Trends Cell Biol.* **29**, 500–513 (2019).
14. J. Cisneros, T. B. Belton, G. C. Shum, C. G. Molakal, Y. C. Wong, Mitochondria-lysosome contact site dynamics and misregulation in neurodegenerative diseases. *Trends Neurosci.* **45**, 312–322 (2022).
15. T. B. Belton, E. D. Leisten, J. Cisneros, Y. C. Wong, Live cell microscopy of mitochondria–lysosome contact site formation and tethering dynamics. *STAR Protoc.* **3**, 101262 (2022).
16. Y. C. Wong, W. Peng, D. Krainc, Lysosomal regulation of inter-mitochondrial contact fate and motility in Charcot-Marie-Tooth Type 2. *Dev. Cell* **50**, 339–354.e334 (2019).
17. Y. C. Wong *et al.*, Mid51/Fis1 mitochondrial oligomerization complex drives lysosomal untethering and network dynamics. *J. Cell Biol.* **221**, e202206140 (2022).
18. L. Langemeyer, F. Frohlich, C. Ungermann, Rab GTPase function in endosome and lysosome biogenesis. *Trends Cell Biol.* **28**, 957–970 (2018).
19. X. M. Zhang, B. Walsh, C. A. Mitchell, T. Rowe, TBC domain family, member 15 is a novel mammalian Rab GTPase-activating protein with substrate preference for Rab7. *Biochem. Biophys. Res. Commun.* **335**, 154–161 (2005).
20. E. R. Peralta, B. C. Martin, A. L. Edinger, Differential effects of TBC1D15 and mammalian Vps39 on Rab7 activation state, lysosomal morphology, and growth factor dependence. *J. Biol. Chem.* **285**, 16814–16821 (2010).
21. K. Onoue *et al.*, Fis1 acts as a mitochondrial recruitment factor for TBC1D15 that is involved in regulation of mitochondrial morphology. *J. Cell Sci.* **126**, 176–185 (2013).
22. K. Yamano, A. I. Fogel, C. Wang, A. M. van der Bliek, R. J. Youle, Mitochondrial Rab GAPs govern autophagosome biogenesis during mitophagy. *Elife* **3**, e01612 (2014).
23. M. Picard, K. White, D. M. Turnbull, Mitochondrial morphology, topology, and membrane interactions in skeletal muscle: A quantitative three-dimensional electron microscopy study. *J. Appl. Physiol.* **1985**, 161–171 (2013).
24. L. Wiemerslage, D. Lee, Quantification of mitochondrial morphology in neurites of dopaminergic neurons using multiple parameters. *J. Neurosci. Methods* **262**, 56–65 (2016).
25. S. K. Bhangoo *et al.*, CXCR4 chemokine receptor signaling mediates pain hypersensitivity in association with antiretroviral toxic neuropathy. *Brain Behav. Immun.* **21**, 581–591 (2007).
26. D. M. Menichella *et al.*, CXCR4 chemokine receptor signaling mediates pain in diabetic neuropathy. *Mol. Pain* **10**, 42 (2014).
27. N. D. Jayaraj *et al.*, Reducing CXCR4–mediated nociceptor hyperexcitability reverses painful diabetic neuropathy. *J. Clin. Invest.* **128**, 2205–2225 (2018).
28. J. M. Kwon *et al.*, Assignment of a second Charcot-Marie-Tooth type II locus to chromosome 3q. *Am. J. Hum. Genet.* **57**, 853–858 (1995).
29. A. M. Valm *et al.*, Applying systems-level spectral imaging and analysis to reveal the organelle interactome. *Nature* **546**, 162–167 (2017).
30. D. Aston *et al.*, High resolution structural evidence suggests the Sarcoplasmic Reticulum forms microdomains with Acidic Stores (lysosomes) in the heart. *Sci. Rep.* **7**, 40620 (2017).
31. J. Fermie *et al.*, Single organelle dynamics linked to 3D structure by correlative live-cell imaging and 3D electron microscopy. *Traffic* **19**, 354–369 (2018).
32. Y. Han, M. Li, F. Qiu, M. Zhang, Y. H. Zhang, Cell-permeable organic fluorescent probes for live-cell long-term super-resolution imaging reveal lysosome–mitochondrion interactions. *Nat. Commun.* **8**, 1307 (2017).
33. Q. Chen *et al.*, Super-resolution tracking of mitochondrial dynamics with an Iridium(III) luminophore. *Small* **14**, e1802166 (2018).
34. S. Khalil *et al.*, A specialized pathway for erythroid iron delivery through lysosomal trafficking of transferrin receptor 2. *Blood Adv.* **1**, 1181–1194 (2017).
35. S. Kim, Y. C. Wong, F. Gao, D. Krainc, Dysregulation of mitochondria–lysosome contacts by GBA1 dysfunction in dopaminergic neuronal models of Parkinson's disease. *Nat. Commun.* **12**, 1807 (2021).
36. J. M. Cioni *et al.*, Late endosomes act as mRNA translation platforms and sustain mitochondria in axons. *Cell* **176**, 56–72.e15 (2019).
37. E. Smirnova, L. Griparic, D. L. Shurland, A. M. van der Bliek, Dynamin-related protein Drp1 is required for mitochondrial division in mammalian cells. *Mol. Biol. Cell* **12**, 2245–2256 (2001).
38. C. R. Schiavon, G. S. Shadel, U. Manor, Impaired mitochondrial mobility in Charcot-Marie-Tooth disease. *Front. Cell Dev. Biol.* **9**, 624823 (2021).
39. S. Zuchner *et al.*, Mutations in the mitochondrial GTPase mitofusin 2 cause Charcot-Marie-Tooth neuropathy type 2A. *Nat. Genet.* **36**, 449–451 (2004).
40. G. W. Dorn, 2nd Mitofusin 2 dysfunction and disease in mice and Men. *Front. Physiol.* **11**, 782 (2020).
41. M. Zaman, T. E. Shutt, The role of impaired mitochondrial dynamics in MFN2-mediated pathology. *Front. Cell Dev. Biol.* **10**, 858286 (2022).
42. O. M. de Brito, L. Scorrano, Mitofusin 2 tethers endoplasmic reticulum to mitochondria. *Nature* **456**, 605–610 (2008).
43. B. M. Woolums *et al.*, TRPV4 disrupts mitochondrial transport and causes axonal degeneration via a CaMKII-dependent elevation of intracellular Ca(2). *Nat. Commun.* **11**, 2679 (2020).
44. G. Landoure *et al.*, Mutations in TRPV4 cause Charcot-Marie-Tooth disease type 2C. *Nat. Genet.* **42**, 170–174 (2010).
45. H. X. Deng *et al.*, Scapuloperoneal spinal muscular atrophy and CMT2C are allelic disorders caused by alterations in TRPV4. *Nat. Genet.* **42**, 165–169 (2010).
46. M. Auer-Grumbach *et al.*, Alterations in the ankyrin domain of TRPV4 cause congenital distal SMA, scapuloperoneal SMA and HMSN2C. *Nat. Genet.* **42**, 160–164 (2010).
47. L. Cantarero *et al.*, Mitochondria–lysosome membrane contacts are defective in GDAP1–related Charcot–Marie–Tooth disease. *Hum. Mol. Genet.* **29**, 3589–3605 (2021).
48. A. Civera-Tregon *et al.*, Mitochondria and calcium defects correlate with axonal dysfunction in GDAP1-related Charcot-Marie-Tooth mouse model. *Neurobiol. Dis.* **152**, 105300 (2021).
49. Y. Gu *et al.*, Mitochondria dysfunction in Charcot Marie Tooth 2B peripheral sensory neuropathy. *Commun. Biol.* **5**, 717 (2022).
50. D. C. Chan, Mitochondrial dynamics and its involvement in disease. *Annu. Rev. Pathol.* **15**, 235–259 (2020).
51. R. Sabouny, T. E. Shutt, Reciprocal regulation of mitochondrial fission and fusion. *Trends Biochem. Sci.* **45**, 564–577 (2020).
52. D. T. Chang, I. J. Reynolds, Mitochondrial trafficking and morphology in healthy and injured neurons. *Prog. Neurobiol.* **80**, 241–268 (2006).
53. M. P. Mattson, M. Gleichmann, A. Cheng, Mitochondria in neuroplasticity and neurological disorders. *Neuron* **60**, 748–766 (2008).
54. F. A. Court, M. P. Coleman, Mitochondria as a central sensor for axonal degenerative stimuli. *Trends Neurosci.* **35**, 364–372 (2012).
55. S. A. Detmer, C. Vande Velde, D. W. Cleveland, D. C. Chan, Hindlimb gait defects due to motor axon loss and reduced distal muscles in a transgenic mouse model of Charcot–Marie–Tooth type 2A. *Hum. Mol. Genet.* **17**, 367–375 (2008).
56. R. Cartoni *et al.*, Expression of mitofusin 2(R94Q) in a transgenic mouse leads to Charcot-Marie-Tooth neuropathy type 2A. *Brain* **133**, 1460–1469 (2010).
57. A. V. Strickland *et al.*, Characterization of the mitofusin 2 R94W mutation in a knock-in mouse model. *J. Peripher. Nerv. Syst.* **19**, 152–164 (2014).
58. P. Bannerman, T. Burns, J. Xu, L. Miers, D. Pleasure, Mice hemizygous for a pathogenic Mitofusin-2 Allele exhibit hind limb/foot gait deficits and phenotypic perturbations in nerve and muscle. *PLoS One* **11**, e0167573 (2016).
59. A. G. Rocha *et al.*, MFN2 agonists reverse mitochondrial defects in preclinical models of Charcot-Marie-Tooth disease type 2A. *Science* **360**, 336–341 (2018).
60. Y. Zhou *et al.*, Restoring mitofusin balance prevents axonal degeneration in a Charcot-Marie-Tooth type 2A model. *J. Clin. Invest.* **129**, 1756–1771 (2019).
61. A. Zuko *et al.*, tRNA overexpression rescues peripheral neuropathy caused by mutations in tRNA synthetase. *Science* **373**, 1161–1166 (2021).
62. Y. Yamada *et al.*, A SARM1/mitochondrial feedback loop drives neuropathogenesis in a Charcot-Marie-Tooth disease type 2A rat model. *J. Clin. Invest.* **132**, e161566 (2022).
63. S. R. Chada, P. J. Hollenbeck, Mitochondrial movement and positioning in axons: The role of growth factor signaling. *J. Exp. Biol.* **206**, 1985–1992 (2003).
64. L. A. Ligon, O. Steward, Movement of mitochondria in the axons and dendrites of cultured hippocampal neurons. *J. Comp. Neurol.* **427**, 340–350 (2000).
65. A. F. MacAskill, J. T. Kittler, Control of mitochondrial transport and localization in neurons. *Trends Cell Biol.* **20**, 102–112 (2010).
66. A. E. Rumora, M. G. Savelieff, S. A. Sakowski, E. L. Feldman, Disorders of mitochondrial dynamics in peripheral neuropathy: Clues from hereditary neuropathy and diabetes. *Int. Rev. Neurobiol.* **145**, 127–176 (2019).
67. S. BasuRay, S. Mukherjee, E. G. Romero, M. N. Seaman, A. Wandinger-Ness, Rab7 mutants associated with Charcot-Marie-Tooth disease cause delayed growth factor receptor transport and altered endosomal and nuclear signaling. *J. Biol. Chem.* **288**, 1135–1149 (2013).
68. D. Colecchia *et al.*, Alterations of autophagy in the peripheral neuropathy Charcot-Marie-Tooth type 2B. *Autophagy* **14**, 930–941 (2018).
69. R. Romano *et al.*, Alteration of the late endocytic pathway in Charcot–Marie–Tooth type 2B disease. *Cell Mol. Life Sci.* **78**, 351–372 (2021).
70. R. Markworth *et al.*, Tubular microdomains of Rab7-positive endosomes retrieve TrkA, a mechanism disrupted in Charcot–Marie–Tooth disease 2B. *J. Cell Sci.* **134**, jcs258559 (2021).
71. W. Peng, Y. C. Wong, D. Krainc, Mitochondria-lysosome contacts regulate mitochondrial Ca(2+) dynamics via lysosomal TRPML1 *Proc. Natl. Acad. Sci. U.S.A.* **117**, 19266–19275 (2020).
72. D. Hoglinger *et al.*, NPC1 regulates ER contacts with endocytic organelles to mediate cholesterol egress. *Nat. Commun.* **10**, 4276 (2019).
73. J. Pijuan *et al.*, Mitochondrial dynamics and mitochondria-lysosome contacts in neurogenetic diseases. *Front. Neurosci.* **16**, 784880 (2022).
74. S. Kim, R. Coukos, F. Gao, D. Krainc, Dysregulation of organelle membrane contact sites in neurological diseases. *Neuron* **110**, 2386–2408 (2022).
75. W. Peng, L. F. Schroder, P. Song, Y. C. Wong, D. Krainc, Parkin regulates amino acid homeostasis at mitochondria–lysosome (M/L) contact sites in Parkinson's disease. *Sci. Adv.* **9**, eadh3347 (2023).